2020 IEEE International Conference on Power Electronics, Drives and Energy Systems (PEDES)

Design and Analysis of Brushless DC Motors for Ceiling Fan Application

Sharankumar Shastri, *Member, IEEE*
Dept. of Electrical Engineering
Indian Institute of Technology Delhi
New Delhi-110016, India
sharan.shastri01@gmail.com

Utkarsh Sharma, *Member, IEEE*
Dept. of Electrical Engineering
Indian Institute of Technology Delhi
New Delhi-110016, India
utkarsh.kota@gmail.com

Bhim Singh, *Fellow, IEEE*
Dept. of Electrical Engineering
Indian Institute of Technology Delhi
New Delhi, India
bsingh@ee.iitd.ac.in

***Abstract*—Permanent magnet brushless DC (PMBLDC) motor-based ceiling fans offer an efficient option to the widely-used single phase induction motor (SPIM) based ceiling fans. A PMBLDCM ceiling fan special features over a SPIM ceiling fan motor include lower input power consumption for the same air-delivery, higher efficiency, efficient speed control, and smaller form factor. This paper deals with the detailed design procedure of a three-phase exterior rotor permanent magnet brushless DC motor for ceiling fan application. The complete procedure is not yet reported for ceiling fans. The analytical design procedure is more computationally efficient than FEA and provides multiple designs covering a wide variety of objectives faster. Detailed analytical design procedure covering the initial sizing, stator, rotor design, and performance assessment is given for a 16-pole, 35 W, 350 rpm surface mounted PMBLDC motor. The results from the analytical design procedure are then validated using 2D FEA software (ANSYS Maxwell).**

Keywords—Permanent magnet brushless DC motors, Ceiling fans, Analytical design, 2D finite element analysis.

I. Introduction

Ceiling fans have significant share of energy consumption as residential loads in tropical and subtropical countries like India and China. The number of ceiling fans sold annually, are about 40.26 million units in India [1] and growing. Conventional single-phase induction motor (SPIM) based ceiling fans consume about 50-80 W of input power for required air delivery of 210-220 m^3/min (CMM). Single phase induction motors for such low power applications have high losses due to a significant requirement of magnetization current and rotor losses, making SPIM-based ceiling fans an unsustainable solution for use in such large numbers. The use of permanent magnet brushless DC (PMBLDC) motor based ceiling fans is an energy-efficient alternative to SPIM based ceiling fans due to their high efficiency and lower input power for the same output air-delivery (or same load requirement). Additional benefits of PMBLDC motor based ceiling fans include constant torque over their complete speed range, lower noise, and efficient speed control through the use of a drive. The use of permanent magnets and power electronics circuitry for the drive, share a significant percentage of the total cost in PMBLDC motor ceiling fans. However, the added costs are compensated by the energy saved.

There has been little literature covered on design and use of PMBLDC motors in ceiling fan application. Several energy-efficient fans are reported in preceding publications [2-10]. Improvement in the efficiency and design of the single phase induction motor have been covered in [2-6]. Sharma and Singh [2] have described the application requirements, need for energy efficiency, and design considerations for single phase induction motor based ceiling fans, using 2D-FEA and two-layer design of experiments (DoE) in detail. Similar work is reported in [3]. A semi-analytical approach using a magnetic circuit based model for the evaluation of performance in SPIM based ceiling fans is reported in [4]. Holik *et al.* [5] have suggested an improvement in the efficiency, through design, of an external-rotor split-phase induction motor, using an external magnetic can. A simple testing method assisted by 2D FEA for SPIM ceiling fan motors, is presented in [6]. Similarly, the performance for an 18-pole permanent split capacitor SPIM ceiling fan motor is derived analytically and tested through 2D-FEA and hardware. The performance improvement of PMBLDC ceiling fan motors is reported in [7-11]. The literature in [7-9] focuses on the improvement in the front-end converters used in the PMBLDCM ceiling fan drives in improving the overall power quality. It is observed that an improved power quality, within rated standards, is obtained for a 30 W ceiling fan motor, for 48V [7] and 110V [8] DC link configurations. An improvement in the efficiency of the PMBLDC ceiling fan motor with a relatively higher motor voltage demonstrated a reduction in input wattage of 4 W in [9]. A single-phase ceiling fan PMBLDC motor has been designed and tested in [10].

This paper presents a step by step methodology for the design of PMBLDC motor for ceiling fan application and attempts to verify the results from the analytical design method with FEA results as closely as possible.

II. Input Specifications for PMBLDC Motor Design

A commercially available ceiling fan PMBLDC motor, shown in Fig. 1, is chosen for this study. The inputs for the analytical design procedure, taking into consideration the electrical and magnetic parameters, are as follows.

A. Material Data

The resistivity of copper (ρ_{Cu}), magnetic flux density (B) versus magnetic field intensity (H) and loss per kg (W/kg, Hz) characteristics of the ferromagnetic material and permanent magnet material used, remanent flux density (B_r) of the magnet, relative recoil permeability (μ_{rec}), the intrinsic coercivity of the magnet (H_c), apparent open circuit MMF of the magnet (H_{ca}), and the density of the magnet (ϱ_m) are the material parameters used in the design of this motor.

B. Geometrical Parameters of Motor

The stator inner and outer diameters (D_{si} and D_{so}), airgap length (l_g), area of airgap (A_g), magnet thickness (l_m), area of the magnet (A_m), pole embrace (α_e), rotor inner and outer diameters (D_{ri} and D_{ro}), the stack height of the motor (L_{stk}), end winding length (L_{end}), number of poles (P), fundamental winding factor (k_{w1}), slot fill factor (SFF), number of turns in

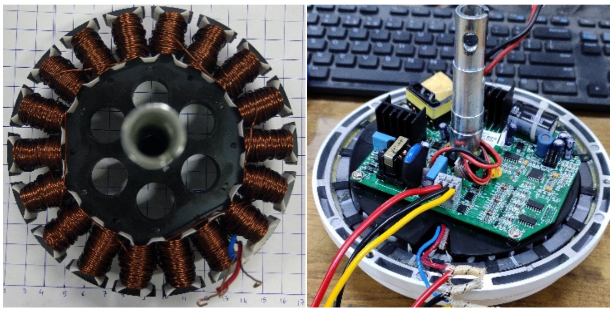

Fig. 1. Schematics of the studied ceiling fan PMBLDC motor

series per phase (N_{ph}), number of coils per phase (N_c), area of the slot (A_{slot}), diameter of the enamelled copper wire (d_{en}), diameter of the bare copper wire (d_{bare}) are the parameters considered in the design of this motor.

C. *Machine Operating Parameters*

Average airgap flux density (B_g), torque per rotor volume (*TRV*), rated current of the motor (I_{ph}) are the operating parameters considered in the design of this motor.

D. *Performance of the Motor*

Average torque (T_{avg}), average power (P_{out}), induced emf/phase (E_{ph}), and efficiency (η_{nom}) are the performance parameters considered in the design of this motor.

III. Preliminary Analysis

Some of the preliminary requirements like mechanical and electrical requirements for the ceiling fan motor application are discussed here.

A. *Mechanical Requirements*

The ceiling fan application requires a low speed operation with two or three blades in the motor. The usual speed range is 200 rpm to 400 rpm. Moreover, the torque of the fan is not more than 1 Nm. Blades for the fan are selected based on the twist angle, and different blades demonstrate different torque-speed characteristics as an effect on the fan load. It is evident that selection of blade also decides the air thrown (CMM), which is a qualitative measure for the fan.

B. *Electrical Motor Requirements*

1) Main dimensions: The overall dimensions of a ceiling fan motor resemble a pancake motor, with smaller stack length and a relatively large bore diameter, due to its placement on the ceiling.

2) Number of pole pairs: The number of poles in a ceiling fan motor are higher, in order to achieve a low synchronous speed at fundamental frequency.

3) Rotor design: The rotor is an exterior surface permanent magnet rotor with core material at its back. For PMBLDC motor ceiling fan, ceramic or ferrite magnets are used for lowering the cost. Ferrite magnets have high resistance to demagnetization and the armature reaction at such a rating is quite low.

4) Winding selection: The number of poles are selected in conjunction with the winding selection, taking into consideration the fundamental winding factor (k_{w1}), synchronous speed (n_s), cogging torque (maximize (LCM[Q_s, $2.p$])), and vibration and noise effects (minimize (HCF[Q_s, $2.p$])). For ceiling fan motors, concentrated nonoverlapped windings are used in both SPIM and PMBLDC motors. For a three-phase ceiling fan PMBLDC motor winding, for the fan close to 350 rpm for full load speed, a couple of winding configurations are chosen, as shown in Table I.

TABLE I. Few Possible Slot-Pole Combinations for PMBLDC Ceiling Fan Motor

Slot/pole combination	**Fundamental winding factor (k_{w1})**	**Synchronous speed (at 50 Hz, rpm)**	**LCM (Q_s, $2.p$)**	**HCF (Q_s, $2.p$)**
12/10	*0.933*	600 rpm	60	2
18/16	***0.945***	**375 rpm**	**144**	**2**

Based on the data presented in Table I, the slot pole combination chosen here (*in bold*) are assessed for further analysis. The winding factors and MMF waveforms with their harmonic spectra are shown in Figs. 2 and 3.

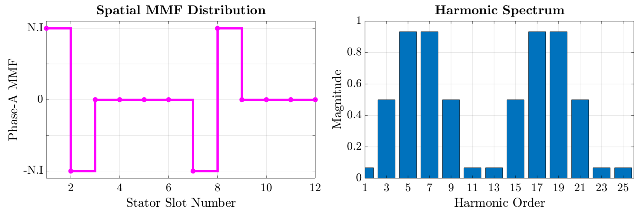

(a) (b)

Fig. 2(a). MMF distribution for 12 slot /10 pole fractional slot concentrated winding, (b) Harmonic spectrum for the same winding.

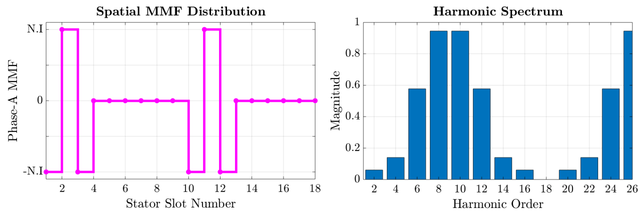

(a) (b)

Fig. 3(a). MMF distribution for 18 slot/16 pole fractional slot concentrated winding, (b) Harmonic spectrum for the same winding.

5) Stator design: The stator uses low loss, high relative permeability steel to reduce core losses at switching frequencies. The steel chosen for this study is JFE steel of the grade 50JN470 (rated loss at 4.7 W/Kg at 50 Hz).

IV. Design Procedure for Ceiling Fan PMBLDC Motor

Initial parameters defined in Fig. 4 and Table II, act as input data to the procedure. The steps for the design of the ceiling fan PM motor are shown in Fig. 5. Further processes are explained in detail in this section.

A. *Initial Sizing*

The machine dimensions considered here are extracted from the motor (Table I). With a known value for inner rotor diameter, D_{ri}, and stack length, L_{stk}, the torque per rotor volume can now be directly calculated from (1). The average current density around the air gap circumference is defined as the electric loading, A (2), whereas the magnetic loading, B, is the average flux density in the air gap, over the rotor surface area (3) [12]. In magnetic loading, a ratio of tooth width to the slot pitch, τ is used [11]. The number of turns can then be determined in (4).

978-1-7281-5672-9/20/$31.00 ©2020 IEEE

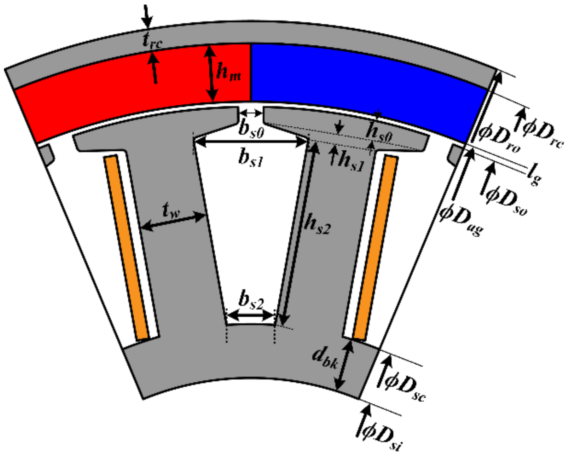

Fig. 4. Design parameters of the one-eighth (1/8th) section of the studied PMBLDC motor.

TABLE II. DESIGN SPECIFICATION OF PMBLDC MOTOR

Parameter	Symbol	Unit	Value
Number of stator teeth	Q_s	--	18
Number of rotor pole pairs	P	--	8
Stator Dimensions	D_{so}	mm	131.7
	D_{si}	mm	66.7
	D_{sc}	mm	79.6
	h_{s0}, b_{s0}	mm	1.97, 3.04
	h_{s1}, b_{s1}	mm	1.41, 13.67
	h_{s2}, b_{s2}	mm	22.7, 5.78
	t_w	mm	8.1
	l_m	mm	7
Air gap length	l_g	mm	0.615
Stack length	L_{stk}	mm	12
Output Power	P_o	W	15
Number of phases	m	--	3
Rated speed	N_{rated}	rpm	350

$$TRV = \frac{T_{rated}}{\pi(0.5\times D_{ri})^2 L_{stk}} \quad (1)$$

$$B = \frac{2\tau B_{tpk}}{\pi} \quad (2)$$

$$A = \frac{TRV\sqrt{2}}{\pi B k_{w1}} \quad (3)$$

$$N_{ph} = \frac{A\pi D_{ri}}{2mI_{ph}} \quad (4)$$

B. Stator Sizing and Winding Parameters

Knowing the dimensions of the stator slots and teeth, the area of all the slots, and subsequently, a single slot area is calculated from (5). The copper area is defined by applying a slot fill factor, SFF, and a current density, J. The cross-section area (CSA) of the copper wire is then calculated as (6).

$$A_{slots} = \pi\left(\frac{(D_{so}-2h_{s0}-2h_{s1})2}{4} - \frac{D_{sc}{}^2}{4}\right) - (Q_s \times h_{s2} \times t_w) \quad (5)$$

$$A_{Cu} = \frac{SFF \times A_{slot}}{3\times 2\times N_{ph}} \quad (6)$$

The stator hosts a fractional-slot concentrated winding (FSCW) configuration, of 18 slots and 16 poles, with a double layer winding. The theory behind the selection of the slot-pole combination is mainly the fundamental winding factor, k_{w1} (7), explained in the preliminary analysis. The value of N_{ph} is previously determined from the electric loading, A. Number of turns per tooth, N_{tooth} is determined, for a concentrated winding can be simply from (8), and is used in determining the cross-section area of the wire.

$$k_{w1} = k_{p1} k_{d1} k_{s1} \quad (7)$$

$$N_{tooth} = \frac{N_{ph}}{Q_s / m} = \frac{A\pi D_{ri}}{2mI_{ph}(Q_s / m)} \quad (8)$$

The resistance of each phase is then calculated, taking into account the length of the winding (including the end winding), turns/phase, N_{ph}, and the cross-section area of the copper conductor in (9).

$$R_{ph} = \frac{\rho \times N_{ph}(2\times L_{stk} + 2\times l_{end})}{A_{Cu}} \quad (9)$$

C. Magnet Sizing

The permanent magnets used in this motor are low-cost ferrite magnets of the grade Y30. The area of magnet per pole, A_m, and area of airgap adjacent to the magnet, A_g, are determined in (10) and (11), respectively. The area of the airgap, A_g, is adjusted to account for the fringing effect by adding $2l_g$ to the main dimensions. A simplified magnetic circuit is used to represent the open-circuit condition of the magnet. The remanent flux in the magnet, ϕ_r is defined as in (12). The magnetic equivalent circuit across one rotor pole is shown in Fig. 6.

$$A_m = \alpha_e \frac{\pi(D_{ri}+l_m)L_{stk}}{2p}; \quad (10)$$

$$A_g = \frac{\pi((D_{ri}-l_g)+(2l_g))(L_{stk}+(2l_g))}{2p} \quad (11)$$

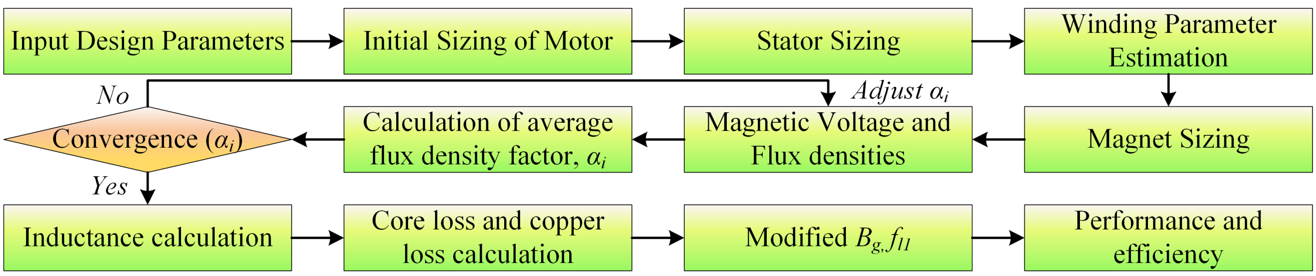

Fig. 5. Flowchart of the implemented design procedure of PMBLDC ceiling fan motor.

978-1-7281-5672-9/20/$31.00 ©2020 IEEE

$$\phi_r = B_r . A_m \tag{12}$$

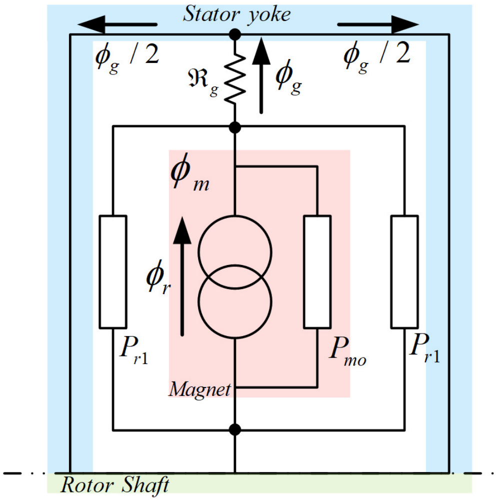

Fig. 6. Magnetic equivalent circuit for one rotor pole, stator and rotor (inverted)

In the equivalent circuit, the reluctances across the stator teeth, stator yoke, and rotor yoke are considered negligible for simplification. The magnet internal leakage permeance, P_{mo} is calculated in (13). Due to the leakage flux outside the magnet, a flux normalization factor, p_{r1}, is introduced (taken here as *0.1*), and the leakage permeance is a multiple of internal leakage and p_{r1} (14). Total permeance, P_m, is the sum of leakage permeance and internal leakage permeance (15). The flux concentration c_ϕ is defined as equal to A_m/A_g.

The air gap flux is determined in (16). Similarly, the airgap flux density, B_g is calculated as (17). The magnet operating flux density can be calculated from (18). The permeance coefficient determines the slope at the magnet's point of operation on the demagnetization curve on open circuit.

$$P_{mo} = \frac{\mu_o \mu_{rec} A_m}{l_m} \tag{13}$$

$$P_{r1} = p_{r1} P_{mo} \tag{14}$$

$$P_m = P_{mo}(1 + p_{r1}) \tag{15}$$

$$\phi_g = \frac{\phi_r}{(1 + P_{mo}(1 + p_{r1})\Re_g)} \tag{16}$$

$$B_g = \frac{c_\phi B_r}{(1 + P_m \Re_g)} \tag{17}$$

$$B_m = \frac{(1 + P_{r1}\Re_g) B_r}{(1 + P_m \Re_g)} \tag{18}$$

D. MMF by Parts

For accurate loss calculation and to determine the operating points of the active parts, accurate calculation of magnetic flux density is important. Due to local saturation in the teeth and yoke, the determination of flux density in these active parts becomes difficult. A term α_i is introduced, which is a coefficient representing the arithmetic average of the air gap flux density of one pole. For sinusoidal flux distribution, the value of α_i is equal to 2/π. For permanent magnet machine, the α_i value is decided from the span of the magnet over the pole pitch, in which the case the peak value of airgap flux density is integrated over the pole pitch, and α_i is greater than 2/π, as shown in Fig. 7.

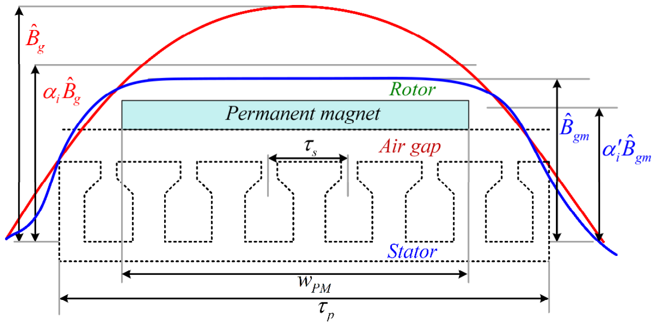

Fig. 7. Pictorial representation of flux density distribution across a pole pitch τ_p (without slotting effects). The red line represents a sinusoidally distributed field. The blue line represents field distribution by a permanent magnet.

Saturation in the teeth leads to flattening of the flux density distribution, and due to an increased reluctance in the stator teeth, therefore, it is important to calculate the effect of saturation (from α_i) on the flux density. A saturation factor, k_{sat} is introduced, which is a function of the magnetic voltages (U_m) across the flux path of one pole. α_i and k_{sat} are related, as shown in (19) and (20) [13].

$$\alpha_i = \frac{1.24 k_{sat} + 1}{1.42 k_{sat} + 1.57} \tag{19}$$

$$k_{sat} = \frac{\hat{U}_{m,s} + \hat{U}_{m,r}}{\hat{U}_{m,g}} \tag{20}$$

For the stator tooth, the incoming flux is a difference between the flux in the tooth region and the flux leaked in the slot region. The apparent flux density in the tooth minus the flux density in the slot portion. The slot pitch at airgap, b_{ds}, slot pitch at b_{s1}, t_{u1s}, and tooth width at b_{s1}, b_{d1s}, are shown in Fig. 8 and defined in (21-23), respectively.

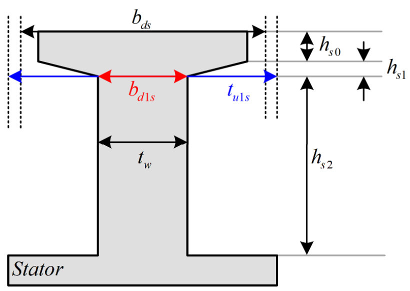

Fig. 8. Stator tooth cut-out showing the dimension used to calculate MMF at various parts of the stator teeth.

$$b_{ds} = \frac{\pi(D_{so} - 2h_{so})}{Q_s} - b_{s0} - 0.0001 \tag{21}$$

$$t_{u1s} = \frac{\pi(D_{so} - 2h_{so} - 2h_{s1})}{Q_s} \tag{22}$$

$$b_{d1s} = \frac{\pi(D_{so} - 2h_{so} - 2h_{s1})}{Q_s} - b_{s1} - 0.0001 \tag{23}$$

An initial estimate of α_i is taken, generally as *2/π*, α_{iu} is defined as the new factor, and a program is written to match

978-1-7281-5672-9/20/$31.00 ©2020 IEEE

the initial estimate to the actual value of α_i as closely as possible. The new updated value of α_i is calculated from k_{sat} till convergence of α_i is close to the actual condition, as shown in Fig. 5. α_i is then used to recalculate the airgap flux density. The peak flux density value can be calculated with an initial estimate of α_i in (24). The apparent flux densities at b_{ds}, B_{dapp}, and at b_{d1s}, B_{da1s}, are calculated from (25) and (26), respectively. S_d (27) is the ratio of slot area to the tooth area calculated to obtain B_d (27).

$$B_{\max} = \frac{\phi_m}{(\alpha_i \times \tau_p \times L_{stk})} \tag{24}$$

$$B_{dapp,bds} = \frac{(L_{stk} + 2(l_g K_{Fe}))\tau_s B_{\max}}{K_{Fe} L_{stk} b_{ds}} \tag{25}$$

$$B_{da1s} = \frac{b_{ds}}{b_{d1s}} B_{dapp,bds} \tag{26}$$

$$S_d = \left(\frac{L_{stk} + 2(l_g K_{Fe})}{L_{stk}} \times \frac{t_{u1s}}{b_{d1s}} \right) - 1 \tag{27}$$

$$B_{dx} = B_{dapp} - S_{dx} \mu_o H_{dx} \tag{28}$$

The magnetic field intensity at tooth opening region, H_{dd} and for the parallel tooth region, H_{d1} are calculated from B_{dapp} and B_{da1s} respectively using the B-H characteristics of the steel used. Finally, the magnetic voltage (MMF) across the tooth, $U_{md,st}$ can be calculated from (29).

$$U_{md,st} = [H_{dd}] \times (h_{s0} + h_{s1}) + \frac{[H_{dd} + H_{d1}] h_{s2}}{2} \tag{29}$$

E. Inductances

The inductance is calculated in two components, the synchronous inductance and the slot leakage inductance, the sum of which is the total phase inductance. The synchronous inductance (30) and the slot leakage inductance (31) are calculated as follows [11].

$$L_s = \frac{6}{\pi} \frac{\mu_o N_{ph}^2 k_{w1}^2 L_{stk} D_{ri}}{2(k_c l_g)} \tag{30}$$

$$L_l = 2pL_{stk} N_c^2 \mu_o (4N_b - n_r) \left(\frac{1}{3} \frac{h_{s2}}{b_{s2}} + \frac{h_{s0} + h_{s1}}{b_{s0}} \right) \tag{31}$$

where, N_b is the slots per pole per phase, N_c is the turns per slot per phase, k_c is the carter coefficient and n_r is the pitch shortening in slots.

F. Calculation of Losses

The core losses are calculated by estimating the masses and volumes of the active parts individually and calculating the loss per kg at their respective operating flux densities.

V. Performance and Efficiency

After calculating all the parameters in the previous section, performance and efficiency can be calculated as follows.

The updated air gap flux density, induced emf per phase, electromagnetic torque, and the total power are determined in (32-35). The losses calculated earlier is used to determine the operating efficiency, η, of the machine (36).

$$B_{g\_new} = \frac{\phi_g}{(A_g \alpha_i)} T \tag{32}$$

$$E_{ph} = 2(2p) N_{ph} \alpha_i \tau_p L_{stk} B_{g\_new} N_{rated} / 60 \tag{33}$$

$$T = 2(2N_{ph} B_{g\_new} L_{stk} (0.5 D_{so} + l_g)) I_{ph} \tag{34}$$

$$P = 2E_{ph} I_{ph} \tag{35}$$

$$\eta = \frac{P}{P + P_{core} + P_{cu}} \times 100\% \tag{36}$$

VI. Results and Discussion

In this section, the results obtained from the analytical procedure are presented and compared with the results obtained from a 2D FEA software. Both the results are compared, and the validity of the design method is tested.

A. Simulation Details

The motor is modeled in a 2D electromagnetic transient solver in ANSYS Maxwell [14]. The total simulation time set has been for 50 ms, with 74794 mesh elements. The excitations given were of current-excited in nature, wherein rectangular current, I_{ph}, is the input source.

B. Results from Described Analytical <ethod

The parameters defined previously are defined for a range of parameters to obtain the results closest to actual results and to also look at the variation of different parameters. Since the simulation has been defined as a current source transient simulation, all the results are plotted with phase current on the y-axis, as demonstrated in Fig. 9.

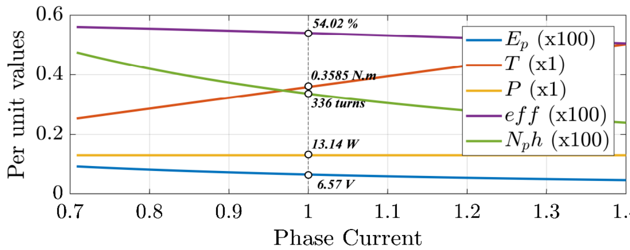

Fig. 9. Trends of different parameters w.r.t phase current (A) observed in the analytical design method.

The results closely matching the FEA results are extracted and are compared in Table III. The flux density plot of the motor obtained from ANSYS Maxwell and the radial flux density are plotted in Fig.10.

TABLE III. Comparison of FEA results with Analytical results

Parameter	Analytical Design	ANSYS Maxwell
Average Torque (N.m)	0.3585	0.3867 [+7.56%]
Average Power (W)	13.1414	14.833 [+11.404%]
Phase Current (A)	1.0	1.0 [+0%]
Induced voltage/phase (V)	6.5707	7.22 [+8.99%]
Airgap flux density (T)	0.3345	0.349 [+4.154%]
Stator resistance/phase (Ω)	0.89	0.9 [+1.11%]
Inductance/phase (H)	3.02e-3	3.5880e-3 [+15.83%]
Efficiency (%)	54.02	--
Simulation time	4.3155 seconds	2.5 hours

978-1-7281-5672-9/20/$31.00 ©2020 IEEE

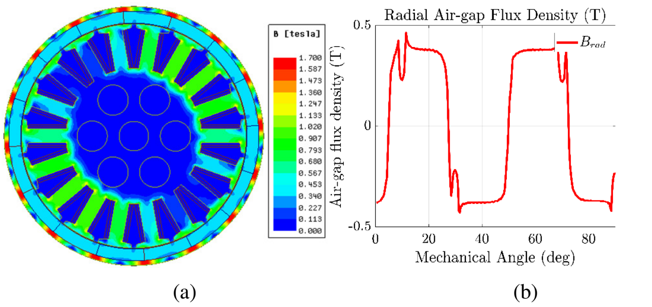

Fig. 10 (a).Flux density plot of the motor obtained from ANSYS Maxwell (at 49.9 ms). (b) Radial flux density plot in the airgap

The results obtained from the FE simulation in ANSYS Maxwell are plotted in Figs. 11 (a-f).

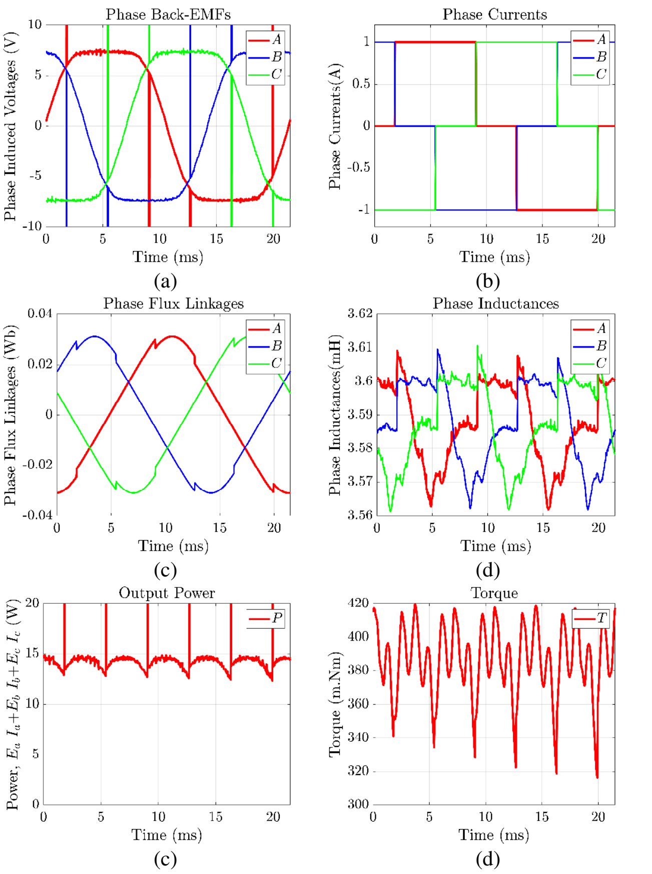

Fig. 11. FEA results showing plots for (a) phase back-EMFs, (b) phase currents, (c) flux linkages, (d) phase inductances, (e) output power, and (f) torque.

Most of the values of various parameters obtained by the analytical design method and from FEA software are in close vicinity, verifying the analytical design method. Major variation obtained with the inductance parameter is primarily due to not including the end winding inductance, which is relatively higher in smaller stack length motors like ceiling fans. The simulation time for the analytical design script is under a minute, while a single FEA transient simulation takes about 2.5 hours (for a medium optimized mesh).

VII. Conclusion

A detailed analytical design procedure for a three-phase exterior rotor permanent magnet brushless DC (PMBLDC) motor for ceiling fan application is presented. The method is well suited for the preliminary sizing of the motor. A commercially available ceiling fan motor has been chosen for this study. Initial sizing, stator parameters, magnet sizing, losses, and performance characteristics are calculated. These calculated results are compared with commercially available 2D FEA software (ANSYS Maxwell). The analytical results and the FE results are compared and are in close vicinity without large error, verifying the design procedure.

Acknowledgments

The authors are extremely grateful to Govt. of India, for funding the FIST project (RP03195) and J.C. Bose fellowship (RP03128).

References

[1] Fourteenth Annual General Meeting, Indian Fan Manufacturers Association, Sep. 2013 [Online]. Available: http://www.indianfan.org/chairmans_message_14-16.html.

[2] U. Sharma and B. Singh, "An Approach to Design of Energy Efficient Single Phase Induction Motor for Ceiling Fans," IEEE International Electric Machines & Drives Conference (IEMDC), San Diego, CA, USA, 2019, pp. 1452-1457.

[3] U. Sharma and B. Singh, "Robust design methodology for single phase induction motor ceiling fan," IET Electric Power Applications, vol. 14, no. 10, pp. 1846-1855, 10, 2020.

[4] H. Saneie and Z. Nasiri-Gheidari, "Performance Analysis of Outer-Rotor Single-Phase Induction Motor Based on Magnetic Equivalent Circuit (MEC)," IEEE Transactions on Industrial Electronics, *Early Access*.

[5] P. J. Holik, D. G. Dorrell, and M. Popescu, "Performance Improvement of an External-Rotor Split-Phase Induction Motor for Low-Cost Drive Applications Using External Rotor Can," IEEE Transactions on Magnetics, vol. 43, no. 6, pp. 2549-2551, June 2007.

[6] U. Sharma and B. Singh, "Suitability Estimation of Ceiling Fan SPIMs Using Locked Rotor and No Load Tests Assisted With FEA," 2020 IEEE International Conference on Power Electronics, Smart Grid and Renewable Energy (PESGRE2020), Cochin, India, 2020, pp. 1-6.

[7] A. Kumar, U. Sharma, and B. Singh, "BLDC Motor Ceiling Fan Using a Bridgeless Isolated PFC SEPIC Converter," 2020 IEEE 9th Power India International Conference (PIICON), SONEPAT, India, 2020, pp. 1-6.

[8] A. Kumar, U. Sharma, and B. Singh, "PMBLDC Motor Based Ceiling Fan Using an Isolated PFC Zeta Converter," 2020 IEEE International Conference on Power Electronics, Smart Grid and Renewable Energy (PESGRE2020), Cochin, India, 2020, pp. 1-6.

[9] S. Manglik, S. Sundeep, and B. Singh, "Brushless DC motor based ceiling fan using buck-boost converter," 2016 IEEE 7th Power India International Conference (PIICON), Bikaner, 2016, pp. 1-6.

[10] M. Fazil and K. R. Rajagopal, "Development of external rotor single-phase PM BLDC motor based drive for ceiling fan," 2010 Joint International Conference on Power Electronics, Drives, and Energy Systems & 2010 Power India, New Delhi, 2010, pp. 1-4.

[11] P. Xie, R. Ramanathan, G. Vakil, and C. Gerada, "Simplified Analytical Machine Sizing for Surface Mounted Permanent Magnet Machines," 2019 IEEE International Electric Machines & Drives Conference (IEMDC), San Diego, CA, USA, 2019, pp. 751-757.

[12] J. R. Hendershot and T.J.E. Miller, *Design of Brushless Permanent Magnet Motors*, Oxford U.K: Oxford 1994.

[13] J. Pyrhonen, T. Jokinen, and V. Hrabovcova, *Design of Rotating Electrical Machines*, 2014 John Wiley & Sons, Ltd, 2014.

[14] *ANSYS Maxwell 2018.0* (2018). ANSYS.